Separation and Purification Technology 176 (2017) 173–183

Contents lists available at ScienceDirect

Separation and Purification Technology

journal homepage: www.elsevier.com/locate/seppur

Mass and heat transfer study in osmotic membrane distillation-crystallization for CO_2 valorization as sodium carbonate

I. Ruiz Salmón *, R. Janssens, P. Luis

Materials & Process Engineering (iMMC-IMAP), Université catholique de Louvain, Place Sainte Barbe 2, 1348 Louvain-la-Neuve, Belgium

ARTICLE INFO

Article history:
Received 10 June 2016
Accepted 9 December 2016
Available online 11 December 2016

Keywords:
Osmotic membrane distillation-crystallization
$Na_2CO_3{\cdot}10H_2O$ production
CO_2 capture
Mass and heat transfer coefficients
Salt concentration

ABSTRACT

Crystallization of $Na_2CO_3{\cdot}10H_2O$ using a membrane contactor is proposed in this work as the last stage of a whole integrated membrane system for the capture of CO_2. The performance of an osmotic membrane distillation-crystallization setup was evaluated, considering the effect caused by the flow rates and the concentration of both the feed and the osmotic solution, as well as the feed temperature, on the mass and heat transfer coefficients. Variation of flow rates and feed concentration did not produce a significant effect on the mass transfer coefficient (except for feed flow rates under 50 mL min^{-1}). On the other hand, decreasing the concentration of the osmotic solution or increasing the temperature led to a decrease in the mass transfer coefficient. Understanding this negative effect of the osmotic solution and temperature on the performance of membrane distillation-crystallization is critical for the further application of this technology in real systems. A deep interpretation is done in this work based on polarization effects and possible membrane wetting. In addition, the resistance-in-series model was applied, which showed the membrane as the main resistance to mass transfer, and the permeate stream to heat transfer.

1. Introduction

An increment of 2.2–3.0 °C in the global average surface air temperature for the period 2071–2100 has been estimated by the Intergovernmental Panel on Climate Change [1], taking as reference the years 1961–1990. This increase will be due to the anthropogenic contribution to the natural climate change, caused by the increment of the global atmospheric concentration of greenhouse gases. Carbon dioxide (CO_2) is the most critical greenhouse gas since its concentration is rising from the pre-industrial era (280 ppm) [2] and has recently reached the value of 400 ppm [3]. About three-quarters of the anthropogenic emissions of CO_2 during the past 20 years come from fossil fuel burning and around 38% of them come from power generation [4]. Hence, the issue must be faced to mitigate the dramatic consequences that are foreseen.

The main current strategy applied to remove the CO_2 from the atmosphere is known as carbon capture and storage (CCS). It consists of the following steps: the CO_2 contained in the flue gases of the power plants (in a post-combustion scenario) is absorbed by a solvent and then it is released in a concentrated form for further compression and storage underground. Absorption using amines is the most mature process to carry out the capture of CO_2 because it presents high capture efficiency and high selectivity of CO_2 at low partial pressures [5]. Thus, the CO_2 reacts with the free radicals of the amines (monoethanolamine –MEA- or similar) in an absorber to produce a "rich" amine that will be further decomposed in a stripper by increasing the temperature to release the CO_2 and reuse the solvent. Nevertheless, the large amount of heat required to regenerate the solvent [6], the operating limitations (foaming, emulsions, etc.) [7] and the toxicity of the amines, underline the need to find other technological alternatives. Furthermore, the transport and storage of the CO_2 into geologic formations, presents some uncertainty about the influence of the capture CO_2 on the geochemical elements (redox condition, microbial activity, etc.) [8].

A competitive alternative to this scenario is the capture of CO_2 as a solid material with the required purity to be used as raw material and avoid new CO_2 emissions in the overall context. To achieve this, CO_2 absorption in a reactive media is proposed. However, two conditions should be satisfied: (i) the chemical absorption between the CO_2 and the absorption liquid should be fast and lead to a product with commercial interest, and (ii) the purity of the final product should meet the industrial necessities. The use of sodium hydroxide (NaOH) provides interesting commercial perspectives. Firstly, it can be obtained as subproduct or waste in different processes such as the treatment of waste streams from Merox towers [9] or glyphosate production [10] leading to a reduction of the

* Corresponding author.
E-mail address: israel.ruizsalmon@uclouvain.be (I. Ruiz Salmón).

http://dx.doi.org/10.1016/j.seppur.2016.12.010
1383-5866/

economic and environmental costs. Secondly, the reaction with CO_2 during the absorption step leads to the formation of sodium carbonate [11], which is widely used (world soda ash production was estimated to be 51.6Mt in 2014 [12]) as raw material in the cement and ceramic industry [13,14]:

$$CO_2 + 2NaOH \rightarrow Na_2CO_3 + H_2O \quad (R1)$$

Once the reaction takes place, sodium carbonate is still in aqueous solution and without commercial value. A last stage of crystallization is needed to obtain the Na_2CO_3as solid product, available for further reuse as raw material. Regarding the species that may be present in the solution, it will depend on the conditions during the absorption, such as composition of the solvent or the reaction time. Secondary reactions leading to the generation of bicarbonate as well as nitrates or sulphates due to the presence of NO_x and SO_2 may take place.

Crystallization is usually applied in the chemical and pharmaceutical industry to separate and/or purify solids from mixed solutions. Nowadays, membrane technology appears as the alternative technology that can replace the conventional crystallizers and evaporators because of its adaptability and low energy consumption in comparison with the conventional technology. This work focuses on the crystallization of Na_2CO_3 using osmotic membrane distillation-crystallization.

The interest of using membrane contactors for crystallization is growing dramatically thanks to its advantages: capacity to independently control the flow rates of the phases involved, known active area, direct scale-up (membrane contactors are modular in design), low energy requirements, and no dragging of drops of solvent because both phases are compartmentalized [8]. In this work, a liquid-liquid configuration will be studied, driving by osmosis and temperature gradients, e.g. difference of vapor pressure [15]. Here, the hydrophobic porous membrane is in contact with two solutions: the feed stream (*i.e.*, solution of Na_2CO_3) in one side and the osmotic solution (concentrated NaCl solution) in the permeate side. The use of NaCl as stripping agent becomes an interesting alternative to conventional separations but also to membrane distillation because (1) its cheap cost (it can be also obtained from the saline recovery treatment leading to zero economy and environmental cost) and (2) the lower energy dependence since it can be performed at room temperature comparing with membrane distillation that usually needs high temperatures. Successful starting results has been already obtained in previous works [14,16] proving the technical viability of this technique.

A step forward is given in this work by studying the effect of the temperature on the mass transfer coefficient, considering the working conditions that could be found in the industry. The study of the temperature acquires an enormous relevance because of the exothermic reaction between CO_2 and NaOH [17], which would lead to a pre-heated feed stream for membrane contactor. The study of the effect of the temperature on the mass transfer coefficient and the evaluation of the heat transfer in the membrane contactor is of utmost importance for the further application in the industry. These aspects are addressed in this work.

2. Experimental

2.1. Chemicals

Deionized water (18.2 MΩ cm^{-1}) was used to prepare the feed and osmotic solutions. Na_2CO_3 (Anhydrous, AnalaRNormapur, 99.5%) was used to simulate the alkaline solution that would be obtained after CO_2 absorption with NaOH. NaCl (AnalaRNormapur, 99.5%) was used as osmotic solution.

2.2. Experimental setup and operation

A hollow fiber membrane contactor (2.5 × 8 Extra-Flow Module™Liqui-Cel®, Membrana GmbH, Germany) was used as membrane crystallizer apparatus. The main specifications are given in Table 1.

The detailed experimental osmotic membrane distillation-crystallization setup is shown in Fig. 1. Here, a membrane contactor acts as a non-selective barrier contacting two solutions: the feed containing Na_2CO_3, whose solute will crystallize due to water permeation though the membrane to the permeate side, and the osmotic solution (NaCl).The influence of the feed temperature was studied, operating the system within the range 20–40 °C. The permeate side was always kept at room temperature.

Fig. 1 shows the schematic diagram of the osmotic membrane distillation-crystallization system. Two peristaltic pumps (Masterflex) circulated the feed stream (Na_2CO_3 solution) and the osmotic stream (NaCl solution) from the reservoirs to the membrane contactor running in counter-current mode. The feed stream circulated inside the lumen side of the membranes and the osmotic stream in the shell side. Several concentrations and flow rates of both streams were studied. The feed stream was prepared with a concentration range from 0 to 200 g l^{-1} and the concentration of the osmotic solution varied from 0 to 300 g l^{-1}. The feed and osmotic flow rates used during the experimentation ranged between 15 and 500 mL min^{-1}, and 50 and 1400 mL min^{-1}, respectively. A first set of experiments were performed at room temperature (20 ± 1 °C). The temperature of the feed and osmotic streams was kept constant by means of water baths (see "D" in Fig. 1).

A second group of experiments was performed at different temperatures between 20 and 40 °C, using Na_2CO_3 feed solutions with concentration from 150 to 200 g L^{-1} and the NaCl osmotic solutions from 200 to 300 g L^{-1}. The volumetric flow rate of the feed stream ranged from 200 to 250 mL min^{-1}; for the osmotic stream, it ranged from 200 to 250 mL min^{-1}.

When crystals were obtained at the bottom of the reservoir, the supersaturated solution was left for 12 h (the bath was set at the same temperature than the feed experimental temperature to avoid crystal phase transition) in order to allow the crystals to grow. Then, filtration of the crystals was done to remove the water from the samples.

The transmembrane flux (J, $m^3\ m^{-2}\ s^{-1}$) of water through the membrane was obtained according to the Eq. (1) by means of weighting of the feed reservoir over time using a balance with precision of ±0.01 g.

$$J(t_i) = -\frac{1}{A}\frac{dV_p}{dt} \approx -\frac{1}{A\rho_{water}}\frac{dw_f}{dt} = -\frac{1}{A\rho_{water}}\frac{w_f(t_{i+1}) - w_f(t_i)}{t_{i+1} - t_i} \quad (1)$$

where V_p (m^3) is the volume of water permeated from the feed solution to the osmotic solution; A (m^2) is the membrane area,

Table 1
Characteristics of the hollow fiber contactor.

Parameters	Data from manufacturer
Module configuration	Hollow fibers
Membrane/potting material	Polypropylene/polyethylene
Fiber i.d/o.d (μm)	240/300
Wall thickness (μm)	40
Effective pore size (μm)	0.04
Porosity (%)	40
Effective fiber length (m)	0.16
Effective membrane surface area (m^2)	1.4
Number of fibers	10,200
Burst strength (bar)	27
Contact angle (°)	112

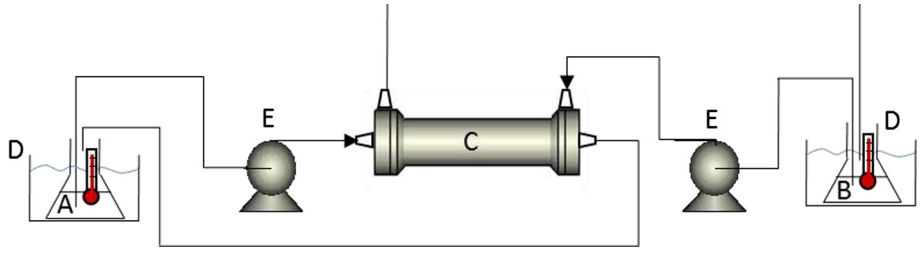

Fig. 1. Osmotic membrane distillation crystallization setup: A, feed solution; B, osmotic solution; C, membrane contactor; E, pumps; D; temperature control system.

ρ_{water} (kg m^{-3}) is the density of water; w_f (kg) is the weight of the reservoir containing the Na_2CO_3 solution at time t_i (s).

The mass transfer from the feed to the osmotic solution is due to the difference of the water activity in the solution in both sides of the membrane. Thus, the principal parameter to evaluate the process is the overall mass transfer coefficient, K_{ov} (m Pa^{-1} s^{-1}), calculated as follows [16,18]:

$$J = K_{ov}(p_f^* a_f - p_p^* a_p) \tag{2}$$

where J is the water flux calculated in Eq. (1); a is the water activity of the feed (f) and osmotic (p) side; and p_f^* and p_p^* are the water vapor pressures (Pa) of the feed and the osmotic solution, respectively.

Both, water activity and water vapor pressure are used at the corresponding operation temperature. Water activity of a pure solution of Na_2CO_3 or NaCl was obtained following the Eq. (3) [18] when the values of the osmotic coefficients corresponding to the salt concentration used were available in the literature. If not, the water activities were calculated using the procedure described by Sandler [19].

$$\varphi = \frac{-1000}{\nu m M} \ln a_w \tag{3}$$

where φ is the osmotic coefficient, ν is the number of ions that the solute molecule dissociates in the solution, m is the molality (mol kg^{-1}), M is the molar mass of the solvent and a_w is the water activity.

The vapor pressure of water (p*) depends on the temperature (T) of the solution and it can be calculated by the Antoine equation (pressure in mm Hg and temperature in °C) [14,20]:

$$p^*(T) = 10^{8.07131 - \frac{1780.68}{233.426+T}} \tag{4}$$

The experimental heat transfer coefficient (U_{exp}, W m^{-2} K^{-1}) was calculated following a semi-empirical procedure in which the heat by convection (Q_{conv}, W m^{-2}) and conduction (Q_{cond}, W m^{-2}) are involved (based on the equation described by Gryta et al. [21]):

$$U_{exp} = \frac{Q_{conv} + Q_{cond}}{\Delta Tln} = \frac{J_w c_P \Delta T_b + \frac{k_{mem}}{\delta}\Delta T_w}{\Delta Tln} \tag{5}$$

where J_w is the permeate flux (kg m^{-2} s^{-1}); c_P is the heat capacity (J kg^{-1} K^{-1}); k_m is the thermal conductivity of the membrane (W m^{-1} K^{-1}) and δ is the membrane thickness (m); $\Delta Tln, \Delta T_b, \Delta T_w$ are the logarithm mean temperature, the difference of temperature among the feed and the osmotic side in the bulk and in the membrane surface, respectively.

2.3. Analytical methods

2.3.1. Microscopy tests

Crystals were examined by means of direct optical microscopy using a microscope Olympus AX70. A calibration was required to clarify the link pixel/distance.

2.3.2. Total Water Fraction (TWF)

The water content of the crystals was analyzed to define the crystalline structure. TWF has to be performed on dried crystals, hence, the remaining water present on the crystals surface coming from the filtration process was dried with a soft tissue. Afterwards, crystals were placed on a chamber for a period of 24 h and finally introduced in an oven at 105 °C for 4 h in order to remove the water contained in the structure.

The water content is determined by means of the following equation, based on the weight of the empty platter ($W_{platter}$), the weight of the platter with crystals before the 24 h in the chamber ($W_{initial}$) and after the oven treatment ($W_{105°C;4h}$):

$$TWF = \frac{w_{initial} - w_{105°C;4h}}{w_{initial} - w_{platter}} \tag{6}$$

3. Modeling of the mass and heat transfer coefficient

According to the resistance-in-series model, three major resistances to mass and heat transfer are considered: the membrane (k_m, h_m), the feed (k_f, h_f) and the osmotic boundary layers (k_p, h_p) located at the membrane surface (see Fig. 2). The serial model expresses the overall mass transfer coefficient (K_{ov}, m s^{-1} Pa^{-1}) and the overall heat transfer coefficient (U, W m^{-2} K^{-1}) by the following expressions [20,22]:

$$J = K_{ov}\Delta P^* = \left[\frac{p_f^*}{k_f} + \frac{1}{k_m} + \frac{p_p^*}{k_p}\right]^{-1}\Delta P^* = [R_f + R_m + R_p]^{-1}\Delta P^* \tag{7}$$

$$Q = U\Delta T_b = \left[\frac{1}{h_f} + \frac{1}{h_m} + \frac{1}{h_p}\right]^{-1}\Delta T_b = [R'_f + R'_m + R'_p]^{-1}\Delta T_b \tag{8}$$

where R represents the three resistances involved (in the feed, membrane and permeate); Q, the total heat flux (W m^{-2}) and ΔT_b (K) the temperature bulk among the feed and the permeate sides.

3.1. Mass transfer coefficients

To describe the mass transfer coefficient inside the fibers (feed side), the following equations are used [20,23]:

$$k_f = \frac{ShD_{Na_2CO_3,water}}{d_i} \tag{9}$$

$$Sh = 0.664 Re^{0.5} Sc^{0.33}\left(\frac{d_i}{l}\right)^{0.33} \tag{10}$$

$$Re = \frac{\rho_f \upsilon_f d_i}{\eta_f} \tag{11}$$

$$Sc = \frac{\eta_f}{\rho_f D_{Na_2CO3,water}} \tag{12}$$

where Sh, Re and Sc stands respectively for Sherwood, Reynolds and Schmidt numbers; d_i (m) is the inside diameter of the fibers;

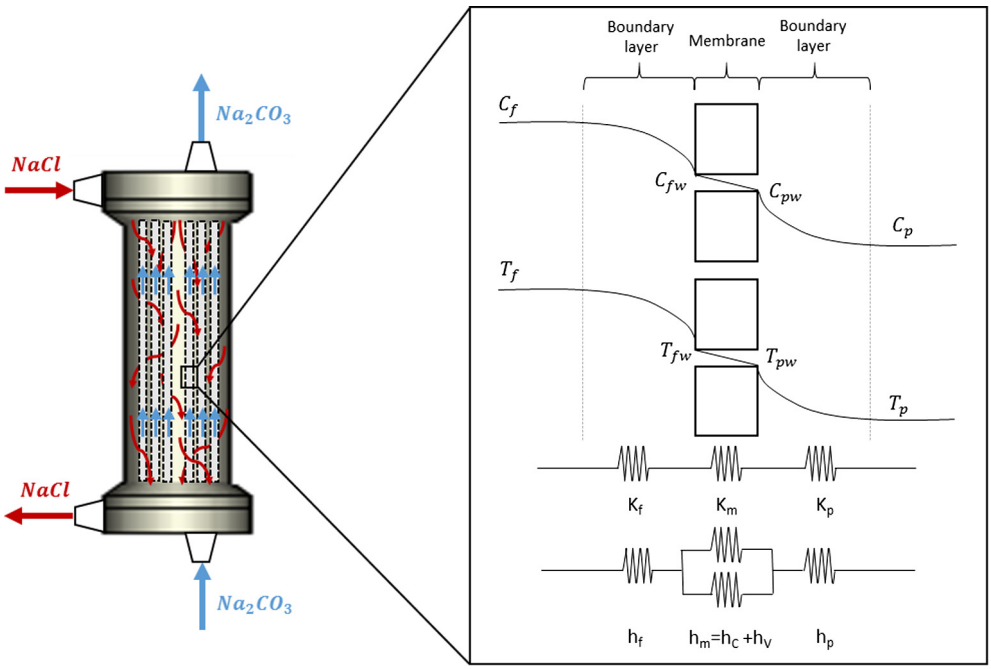

Fig. 2. Counter-current mode in osmotic membrane distillation (left) and mass and heat transfer resistances (right).

ρ (kg m^{-3}) and η (Pa s), the density and the viscosity of the solution, respectively; v (m s^{-1}), the velocity of the fluid through the fibers and $D_{Na_2CO3,water}$ (m^2 s^{-1}) is the diffusivity of Na_2CO_3 in water.

The mass transfer coefficient at the shell side (osmotic solution) is calculated from [20,23]:

$$k_p = \frac{ShD_{NaCl,water}}{d_h} \tag{13}$$

$$Sh = 5.8\left(\frac{d_{h(1-\phi)}}{l}\right)Re^{0.6}Sc^{0.33} \tag{14}$$

$$Re = \frac{\rho_p v_p d_h}{p} \tag{15}$$

$$Sc = \frac{\eta_p}{\rho_p D_{NaCl,water}} \tag{16}$$

where l (m) is the length; d_h (m), the hydraulic diameter and ϕ is the packing fraction of the fibers in the shell.

Regarding the mass transfer coefficient in the membrane, it is calculated from [20,23]:

$$k_m = \frac{1}{RT}\left(\frac{D_w^k D^\circ_{w-a}}{D^\circ_{w-a} + p_a D_w^k}\right)\left(\frac{M}{\delta}\right) \tag{17}$$

$$D_w^k = \frac{2\varepsilon r_p}{3\tau}\sqrt{\frac{8RT_{avg}}{\pi M}} \tag{18}$$

$$D^\circ_w(T) = -2.775\ 10^{-6} + 4.479\ 10^{-8}T + 1.656\ 10^{-10}T^2 \tag{19}$$

where D_w^k is the water Knudsen diffusion; D°_w, the water air diffusion; T, the temperature along the membrane; p_a is the partial pressure of air in the pore (it is assumed p_a = 101,325 Pa); τ, the tortuosity of the membrane; $\in$, the porosity of the membrane; δ, the thickness of the membrane and r_p, the radius of the pores.

3.2. Heat transfer coefficients

The heat transfer coefficients (h, W m^{-2} K^{-1}) and the temperature polarization coefficient (*TPC*) are calculated from correlations [21,24–26]. The calculation of the heat transfer coefficients in the feed (h_f) and permeate (h_p) corresponds to Eqs. (20)–(22):

$$h = \frac{Nuk_{fluid}}{d} \tag{20}$$

$$Nu = 1.86\left(RePr\frac{d}{l}\right)^{0.33}\left(\frac{\eta}{\eta_w}\right)^{0.14} \tag{21}$$

$$Pr = \frac{C_p\eta}{k_{fluid}} \tag{22}$$

where Nu and Pr are the Nussel and Prandtl numbers, respectively; k_{fluid} is the thermal conductivity of the fluid (W m^{-1} K^{-1}), d (m) is d_i and d_h for the feed and the osmotic side, respectively; η and η_w are the viscosity of the solution (feed or osmotic solution) and the water, respectively; C_p is the heat capacity (J kg^{-1} K^{-1}) and k_{fluid} is the thermal conductivity of the fluid (W m^{-1} K^{-1}).

The calculation of the heat transfer through the membrane by conduction (h_c) and vapor movement (h_v), and the temperature polarization coefficient (*TPC*) corresponds to Eqs. (23)–(28):

$$h_c = \frac{k_{mem}}{\delta} = \frac{\in k_g + (1-\in)k_s}{\delta} \tag{23}$$

$$h_v = \frac{J_w\Delta H_v}{\Delta T_w} \tag{24}$$

$$\Delta T_w = T_{fw} - T_{pw} \tag{25}$$

$$T_{fw} = T_f - (T_f - T_p)\left(\frac{\frac{1}{h_f}}{\frac{1}{h_c+h_v} + \frac{1}{h_f} + \frac{1}{h_p}}\right) \tag{26}$$

$$T_{pw} = T_p + (T_f - T_p)\left(\frac{\frac{1}{h_p}}{\frac{1}{h_c+h_v} + \frac{1}{h_f} + \frac{1}{h_p}}\right) \tag{27}$$

$$TPC = \frac{\Delta T_w}{T_f - T_p} \quad (28)$$

where k_{mem}, k_g, k_s are the thermal conductivity of the membrane, the air and the solid phase of the membrane, respectively; ΔH_v is the latent heat of vaporization (J kg^{-1}); ΔT_w is the temperature difference (K) among the temperature near the membrane wall in the feed (T_{fw}) and the permeate side (T_{pw}).

4. Results and discussion

The influence of three main variables, *i.e.*, concentrations and flow rates of both feed and osmotic solutions and feed temperature, on the water flux through the membrane was studied according to the experimental conditions defined in Section 2.2. Results are shown in the next sections.

4.1. Influence of the concentration on the mass transfer coefficient

Different concentrations at both the feed and the osmotic sides were studied in order to evaluate their effect on the transmembrane flux. A slight decrease in fluxes was observed during the first minutes of each experiment (see Fig. A1 in Appendix) and therefore this startup period (20–30 min) was not used for the calculation of the average transmembrane flux. Figs. 3–9 represent thus the experimental data when steady state conditions were reached (transmembrane fluxes are plotted in mL m^{-2} min^{-1}). The effect of concentration/dilution of the feed/osmotic solutions during the experiments due to the transfer of water through the membrane was neglected since the volumes of both solutions were large enough to minimize this effect.

Three kind of experiments were done: (i) experiments using pure water as feed solution in order to evaluate how the NaCl concentration of the osmotic solution (permeate side) affects the system (NaCl concentration varied from 100 to 300 g L^{-1}); (ii) experiments with a feed solution containing 100 g L^{-1} Na_2CO_3 (NaCl concentration varied from 100 to 300 g L^{-1}) and, (iii) experiments in which the concentration of the osmotic solution is kept constant at 300 g L^{-1} NaCl and the concentration of the carbonate solution is varied from 100 to 200 g L^{-1} Na_2CO_3. The flow rates of the feed and osmotic solutions were 300 mL min^{-1} and 450 mL min^{-1}, respectively. The results of transmembrane flux and the overall mass transfer coefficient calculated using Eq. (2) are plotted in Figs. 3 and 4, respectively. Values are in the range

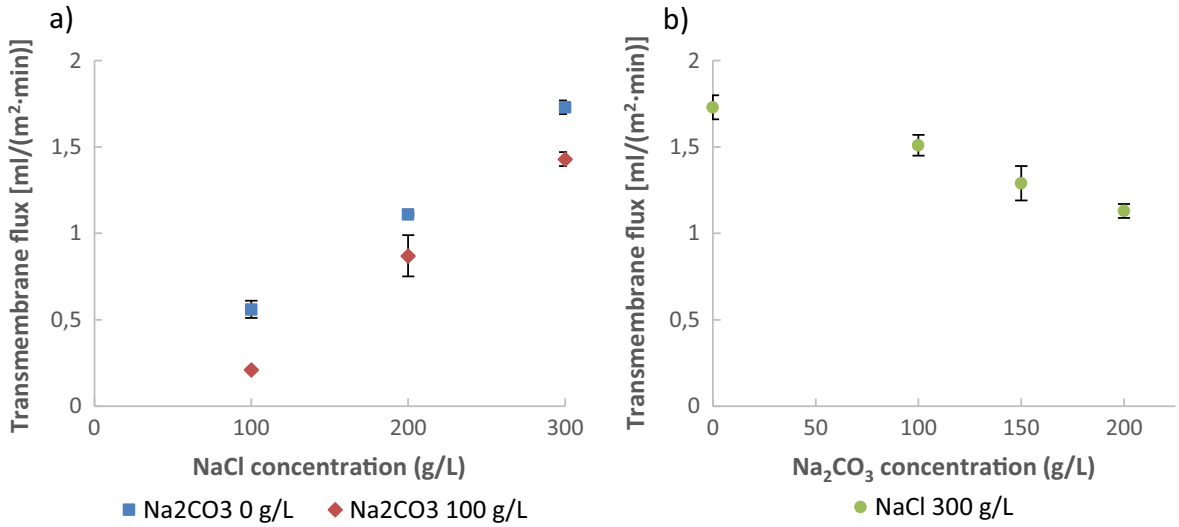

Fig. 3. Transmembrane flux as a function of the concentration of Na_2CO_3 and NaCl solutions. Na_2CO_3 and NaCl flow rates are 300 and 450 mL min^{-1}, respectively.

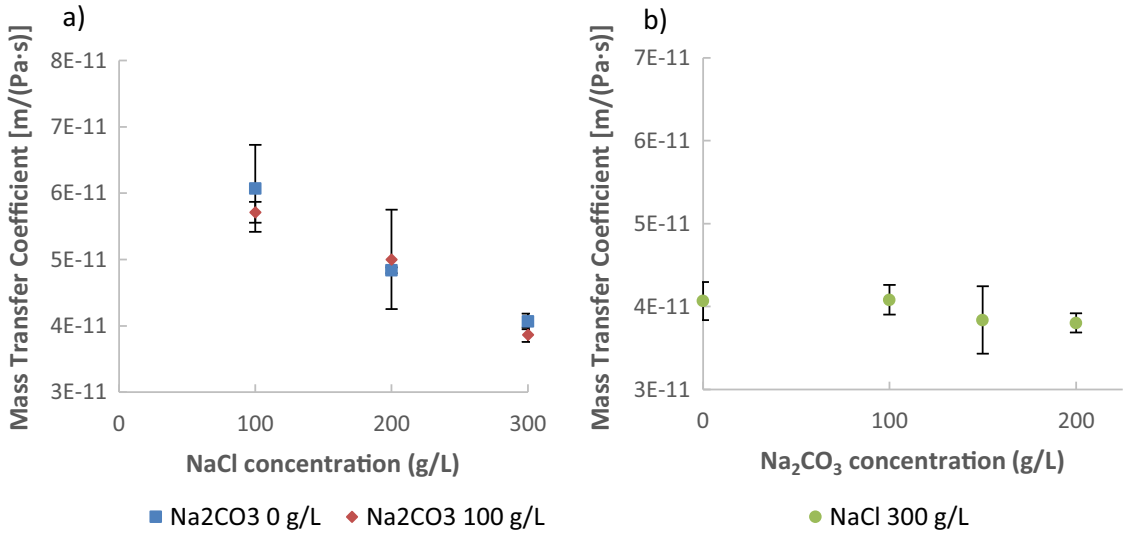

Fig. 4. Mass transfer coefficient as a function of the concentration of Na_2CO_3 and NaCl solutions. Na_2CO_3 and NaCl flow rates are 300 and 450 mL min^{-1}, respectively.

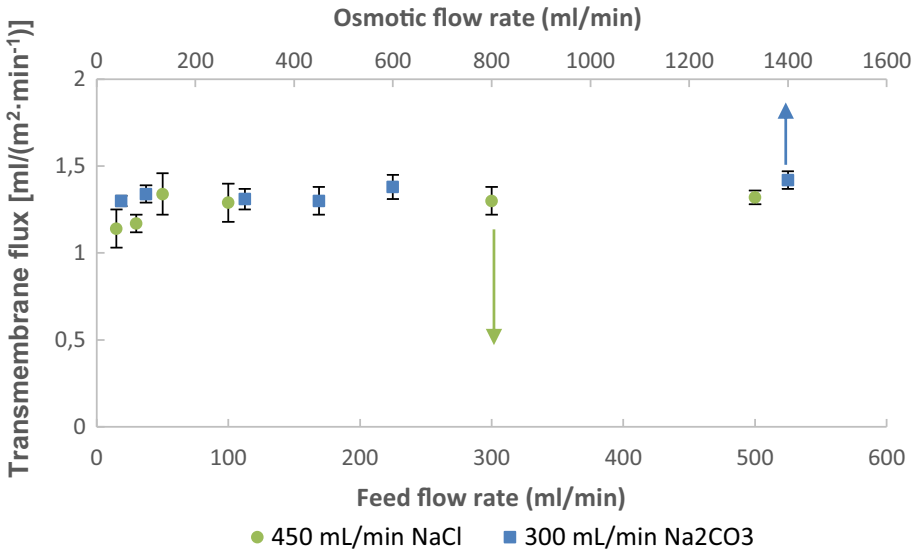

Fig. 5. Transmembrane flux as a function of the feed and osmotic flow rates. Na_2CO_3 and NaCl concentration are 150 and 300 g L^{-1}, respectively.

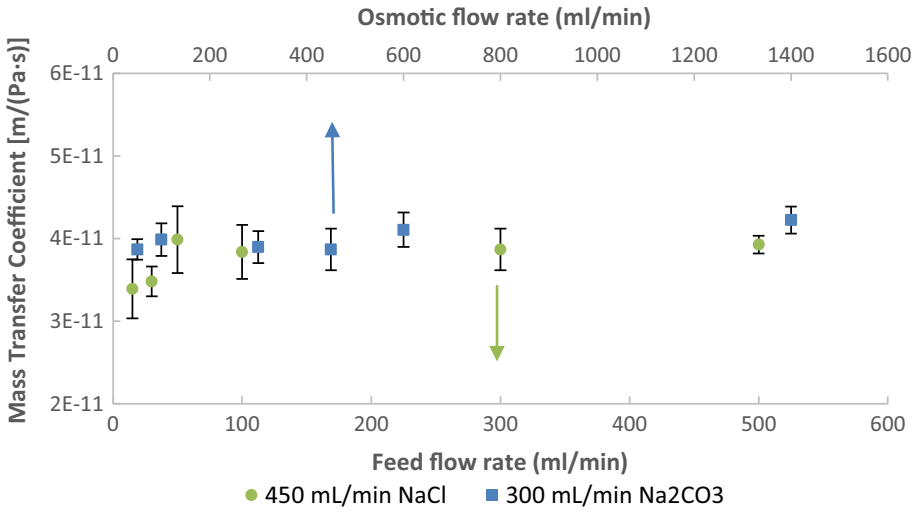

Fig. 6. Mass transfer coefficient as a function of the feed and osmotic flow rates. Na_2CO_3 and NaCl concentration are 150 and 300 g L^{-1}, respectively.

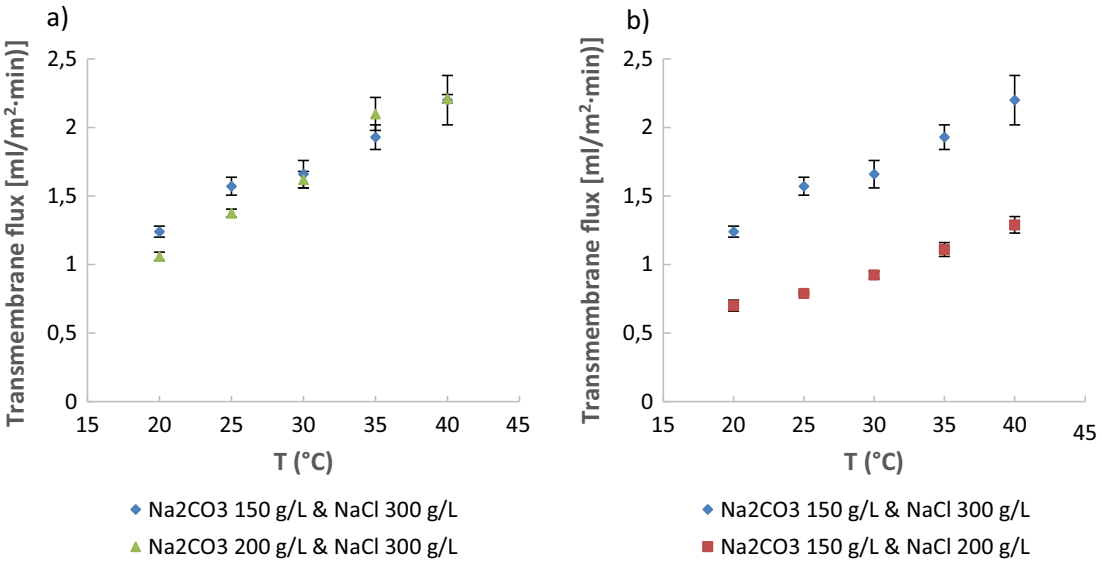

Fig. 7. Transmembrane flux as function of the feed temperature. Feed and osmotic flow rates are 250 mL min^{-1}.

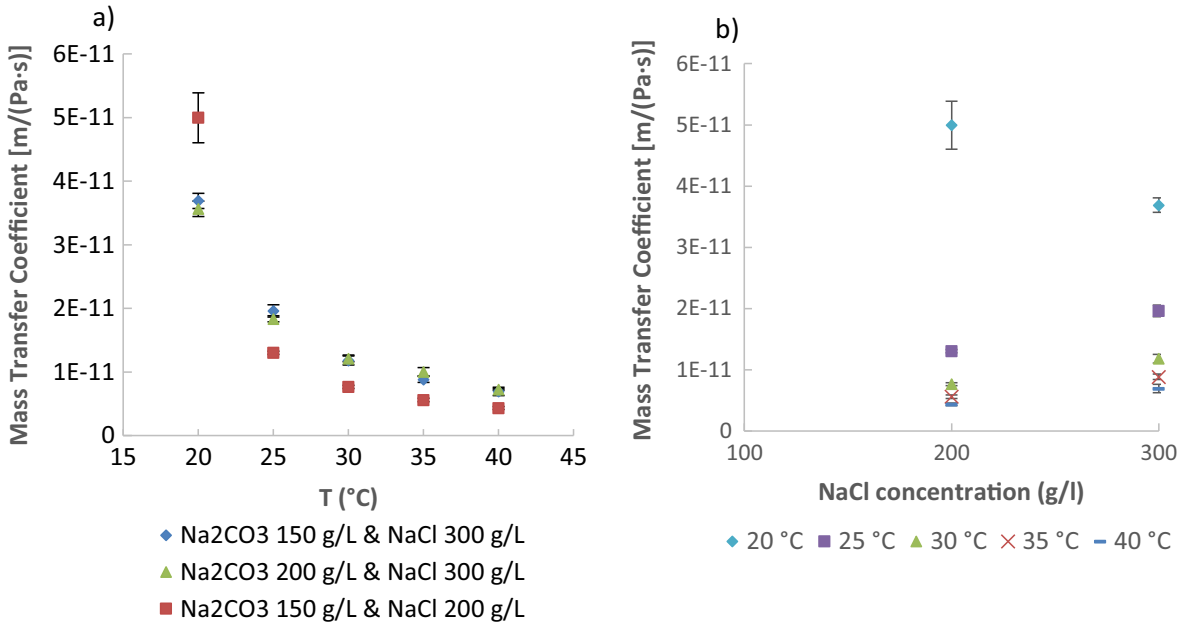

Fig. 8. Mass transfer coefficient as function of the feed temperature (left) and NaCl concentration (right). Feed and osmotic flow rates are 250 mL min^{-1}. Na_2CO_3 concentration in b) is 150 g L^{-1}.

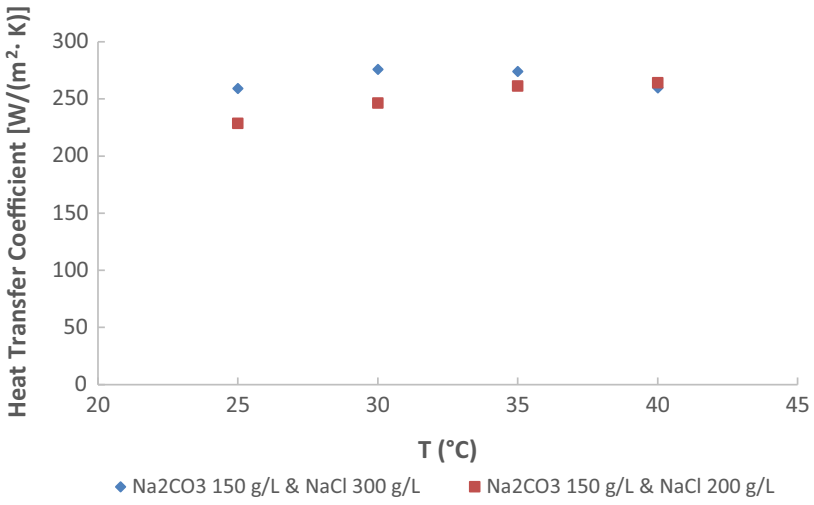

Fig. 9. Heat transfer coefficient as function of the feed temperature. Feed and osmotic flow rates are 250 mL min^{-1}.

of those obtained in previous works with a minimodule contactor [14,16,18,20].

As expected, fluxes are higher when pure water is used as feed solution and when the osmotic concentration is increased. This happens because of the water activities of the solutions (Fig. A2 in Appendix): the higher the concentration, the lower the activity (and smaller the driving force). In summary, taking into account Eq. (2), fluxes increase when the concentration of the NaCl also does (Fig. 3a) or when the concentration of Na_2CO_3 decreases (Fig. 3b). The dependence of the transmembrane flux on the osmotic concentration is stronger because the water activity dependence on concentration is higher (it is related to the higher ionic strength of the osmotic ions than the feed ions present in solution). Hence, a large variation in the fluxes can be observed when the influence of the NaCl concentration is evaluated.

Regarding the mass transfer coefficients (Fig. 4), an important decline was observed with the increase of the osmotic concentration (Fig. 4a). As mentioned above, the higher the osmotic concentration, the higher the driving force for water evaporation and, consequently, the water removal at the membrane surface should also increase. This would normally lead to an overall mass transfer coefficient that is constant (no dependent on the concentration) if the flux increases in the same ratio as the driving force, as it happens when the concentration of Na_2CO_3 in the feed stream is varied (Fig. 4b). However, the experimental results show a different trend on the effect of the osmotic solution. A decrease of the overall mass transfer coefficient is observed with the increase of concentration, which indicates that a higher driving force is not leading to the expected increase of flux. This result was also observed by Li et al. [19]. Concentration polarization may be the cause of this loss of performance. As observed above, the highest transmembrane flux is reached when the highest concentration of NaCl is used. Thus, it is evident that increasing the concentration of the osmotic solution is desired to increase the flux but the effect is hindered by a polarization phenomenon that leads to a lower flux than expected. This loss of performance is more significant at higher concentrations of NaCl, thus, using the highest concentration is not the optimal condition in terms of membrane performance.

In order to determine if concentration polarization can be minimized by increasing the turbulence of the feed and osmotic streams, the study of the effect of flow rate was carried out and it is presented in the next section.

4.2. Influence of the flow rates on the mass transfer coefficient

The transmembrane flux as a function of the flow rates of both solutions in the shell and lumen sides are plotted in Fig. 5. Different flow rates of the Na_2CO_3 solution (15–500 mL min^{-1}) and the NaCl solution (50–1400 mL min^{-1}) were considered. The feed and osmotic solutions had a concentration of 150 and 300 g l^{-1}, respectively. The osmotic flow rates for the range studied reveals no influence on the transmembrane fluxes; the average overall mass transfer coefficient takes a value of 3.98×10^{-11} m s^{-1} Pa^{-1} ($\pm 1.48 \times 10^{-12}$ m s^{-1} Pa^{-1}). On the other hand, results indicate a slight decrease in the transmembrane flux when the feed flow rate is lower than 50 mL min^{-1}. The low feed velocities, which result in Reynolds numbers lower than 100, can reduce the flux due to the presence of a boundary layer on the surface membrane caused by a polarization phenomenon [25,26]. In polarization, a gradient of concentration and/or temperature exists from the bulk fluid to the membrane surface due to the lack of turbulence. If this effect becomes stronger, scaling may be produced because crystal deposition on the membrane surface [24,27,28] or spontaneous wetting of the membrane may appear causing an increment of the overall resistance to mass transfer [26]. This polarization effect can be better observed when the influence of the flow rate on the mass transfer coefficient is evaluated (Fig. 6). Only below a feed velocity of 50 mL min^{-1}, a decrease in the mass transfer coefficient occurs. Above this value, no relevant differences are observed, with an average overall mass transfer coefficient of $3.89 \times 10^{-11} \pm 7.28 \times 10^{-13}$ m s^{-1} Pa^{-1}.

Therefore, two conclusions may be inferred from this interpretation: (i) a polarization phenomenon appears in the feed side when the flow rate is lower than 50 mL min^{-1}. Higher flow rates are thus required in the contactor; and (ii) the flow rate does not have a significant effect on the mass transfer in the osmotic side. In the previous section, concentration polarization had been considered as the phenomenon that is decreasing the mass transfer coefficient at higher osmotic concentrations. However, increasing the flow rate does not seem to have any kind of effect, hence, there is not enough turbulence to decrease the resistance in the osmotic side. In addition to this, membrane wetting enhanced at higher concentrations may also contribute to the fact that the transmembrane flux does not increase proportionally to the driving force. In any case, a compromise between low flux-high performance and high flux-low performance will have to be considered taking the cost as a major decisive parameter.

4.3. Influence of the temperature on the mass and heat transfer coefficient

The influence of the feed temperature is a key step in the consideration of membrane distillation-crystallization as potential technology for the crystallization of sodium carbonate. The coupled effect of temperature and NaCl concentration is studied in this section in order to advance in the state-of-the-art of this technology.

The effect of the feed temperature, ranging from 20 to 40 °C, on the transmembrane flux is shown in Fig. 7. In these experiments, a new driving force is incorporated: the vapor pressure difference created by the temperature difference across the membrane. Thus, the evaporation rate increases when the feed temperature also does and higher fluxes are then reached. At this point, the three factors (*i.e.,* feed temperature, concentration of the feed solution and concentration of the osmotic solution) were evaluated at several temperatures. The effect of increasing the temperature can be observed in Fig. 7a and b. When the concentration of the feed solution is varied (Fig. 7a), a slight effect on the flux is observed coming from this driving force but only at low feed temperatures (20 and 25 °C), while this influence almost disappears at higher temperatures. This is due to the lower strength of the ions in the feed solution and therefore, the driving force coming from the variation of the sodium carbonate concentration is negligible compared with the one caused by the temperature difference. On the other hand, a variation of the osmotic concentration (Fig. 7b) showed a larger difference between two experimental conditions. The increment in NaCl concentration produces a sharp decrement in the water activity, as collected Fig. A2, and therefore higher fluxes are reached. It can be seen that parallel lines are obtained when the temperature is varied which means that osmotic and temperature effects are independent and no synergy exists between them.

Regarding the mass transfer coefficients, plotted in Fig. 8, a dramatic decrease was observed when the feed temperature increased (Fig. 8a). In this case, temperature polarization explains that mass transfer is hindered. Temperature polarization coefficient (TPC) is defined in the Eq. (28) as the ratio between the temperature difference of the feed and osmotic side at the membrane surface and the bulk solutions. The value of TPC approaches zero when the system is impeded by large boundary layer resistances, *i.e.*, high degrees of temperature and/or concentration polarization; if the value of TPC is close to the unity, the process is controlled by the mass transfer [25,26,29]. However, it should be noted that concentration polarization is practically neglected compared to temperature polarization when non-volatile solutes, as sodium carbonate, are considered [29,30]. Thus, the TPC average value, calculated by Eqs. (23)–(28) in an iterative process, is lower than 0.13 confirming that a heat transfer resistance is the main factor involved. Moreover, Fig. 8b corroborates this. A decrease of the mass transfer coefficient over the osmotic concentration is observed at room temperature. But, when feed temperature is raised, a sharp decrease on the mass transfer coefficient is observed due to the temperature polarization effect, much larger than the one produced by the effect of concentration.

These results, as mentioned previously, inferred that the best working conditions for the whole system and for the membrane are not the same. The best conditions for both cases are summarize in Table 2. Thus, if the goal is to obtain the highest fluxes (and therefore the lowest area of membrane), the best conditions are low concentration in the feed, high concentration in the osmotic solution, and high feed temperature. Nevertheless, the highest performance of the membrane contactor (the highest mass transfer coefficient) is found with low feed and osmotic concentrations and feed at room temperature. In both cases, the flow rates of the feed solution should be higher than 50 mL min^{-1}. Therefore, the selection of the optimal working conditions becomes essential and from an economic point of view, investment costs (*i.e.,* area) and operating costs (*i.e.,* raw material, energy) play a fundamental role in the discussion.

The heat transfer coefficient was calculated using the Eqs. (5) and (23)–(27) and results are plotted in Fig. 9. It can be observed

Table 2
Optimal working conditions for the osmotic membrane distillation-crystallization system and for the membrane contactor.

Case	Concentration [g L^{-1}]		Flow rates [mL min^{-1}]		Feed temperature [°C]
	Feed	Osmotic	Feed	Osmotic	
Maximizing flux	100	100	>50	>50	40
Maximizing performance	100	300	>50	>50	20

that high concentration of the NaCl solution influences slightly the heat transfer but this effect disappears as soon as the feed temperature is increased above 35 °C.

4.4. Resistance-in-series model

The resistance-in-series model was applied in order to characterize theoretically the mass and heat transfer on the osmotic membrane distillation-crystallization plant.

The mass transfer coefficients of the feed and osmotic side and the membrane were calculated using the Eqs. (2), (7) and (9)–(19). Table 2 shows as example the results for one of the experiments made. It can be seen that the coefficients in both sides of the membrane were several orders of magnitude larger than the mass transfer coefficient obtained for the membrane. The membrane presented thus the main limitation to the mass transfer representing 90.7% of the total resistance. Meanwhile, resistances of the feed and osmotic solutions were 3.6 and 5.7%, respectively. In summary, it was found that the membrane is the main limiting factor to the mass transfer.

A comparison between the theoretical overall mass transfer coefficient obtained from Eq. (7) and the experimental one obtained using Eq. (2) was performed aiming at (i) confirming the experimental results by means of a mathematical model and (ii) therefore, providing an useful tool for further simulation. Thus, both Table 3 and Fig. A3 reveals that the model applied for calculation fitted with high accuracy with the experimental results obtained in the laboratory (differences smaller than 11.5%). The differences higher than 10% were found in those values for feed velocities lower than 50 mL min^{-1}. This leads to the conclusion that the real mass transfer mechanisms are affected by concentration polarization are not well described by the mathematical model.

On the other hand, Table 4 collects the theoretical analysis of the heat transfer coefficients and heat fluxes. The overall heat transfer coefficient (U) was calculated as the sum of the partial resistances (from the feed -h_f- and osmotic -h_p- boundary layers and the membrane -h_m-). Table 4 shows that the overall heat transfer coefficients keep the same value for the feed temperature range studied. Thus, for 200 and 300 g L^{-1} of NaCl concentration, U takes a value of 256.47 ± 0.16 and 262.05 ± 0.17 W m^{-2} K^{-1}, respectively.

It can be observed that heat fluxes, calculated by Eq. (8), increase with the osmotic concentration and the feed temperatures. Thus, the main resistance to the heat transfer came from the permeate (76.4–77.2% for the range studied), followed by the membrane (12.4–12.7%) and the feed (10.3–10.9%).

Simultaneously, a comparison between both theoretical and semi-empirical heat transfer coefficients was made and results plotted in Fig. A4 reveals high accuracy for the range studied.

4.5. Crystal characterization

The pictures of crystals obtained by direct optical microscopy tests are shown in Fig. 10. Left- side image shows the crystals after the filtration step while the central image shows the crystalline structure after drying at room temperature. The concentric circles

Table 3
Mass transfer coefficients. Conditions: Na_2CO_3 concentration and flow rate are 150 g L^{-1} and 200 mL min^{-1}. NaCl concentration and flow rate are 200 g L^{-1} and 200 mL min^{-1}, respectively. Room temperature.

k_f (m s^{-1})	k_p (m s^{-1})	k_m (m s^{-1} Pa^{-1})	$k_{overal(theoretical)}$ (m s^{-1} Pa^{-1})	$k_{overal(experimental)}$ (m s^{-1} Pa^{-1})	*Error* (%)
2.64×10^{-6}	1.66×10^{-6}	4.48×10^{-11}	4.06×10^{-11}	4.99×10^{-11}	2.29

Table 4
Heat transfer coefficients. Conditions: Na_2CO_3 concentration and flow rate are 150 g L^{-1} and 250 mL min^{-1}, respectively. NaCl flow rate is 250 mL min^{-1}.

Experiment conditions	T_f (°C)	h_f (W m^{-2} K^{-1})	h_p (W m^{-2} K^{-1})	h_m (W m^{-2} K^{-1})	U (W m^{-2} K^{-1})	Q (W m^{-2})
[NaCl] = 200 g L^{-1}	20	332.65	2060	2060	255.75	0
	25	332.65	2060	2060.27	256.53	1282.64
	30	332.65	2060	2060.32	256.54	2565.40
	35	332.65	2060	2060.38	256.86	3852.95
	40	332.65	2060	2060.44	256.65	5133
[NaCl] = 300 g L^{-1}	20	342.09	2060	2060	261.30	0
	25	342.09	2060	2060.52	262.11	1310.55
	30	342.09	2060	2060.55	262.12	2621.22
	35	342.09	2060	2060.64	262.46	3936.90
	40	342.09	2060	2060.73	262.24	5244.76

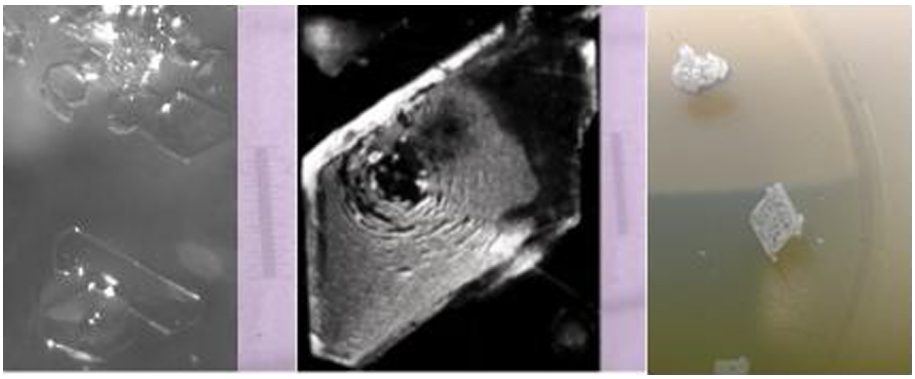

Fig. 10. Micrograph of crystals after filtration (left) and after drying (center) with 16× magnification. The calibration line represents 1 mm. Right image shows the white powder on the crystal surface after drying, corresponding to a different phase of the crystal.

Table 5
Theoretical TWF for different crystals.

Crystal	$TWF_{theoretical}$ (%)
Na_2CO_3	0
$Na_2CO_3{\cdot}H_2O$	14.5
$Na_2CO_3{\cdot}7H_2O$	54.3
$Na_2CO_3{\cdot}10H_2O$	62.9
Average or 6 samples (this work)	65.6 ± 0.7

on the crystal surface could not be seen before the drying step. This is due to the water layer evaporation during the drying step and, as a result, a different phase layer at the crystal surface appeared (see right-side picture in Fig. 10). Efflorescence (i.e., total or superficial conversion of a mass into powder caused by the loss of water) may explain this phenomenon. The crystals formed a residue of lower hydrates (mainly the monohydrate form) as a consequence of the drying [31].

The amount of water in the crystals was also studied by means of the Total Water Fraction method, according to Eq. (6). Table 5 represents the values of the theoretical TWF in function of the type of crystals, *i.e.*, the amount of water molecules in the carbonate crystals, as well the value obtained in this work.

It was expected to obtain decahydrate carbonate due to the conditions during the experiment, taking into account the typical diagram phase (concentration vs temperature) [32]. Regarding the results presented in Table 5, the average of six samples shows 65.6% of water content, about 4.3% more water than in the theory, but still, it can be confirmed the production of $Na_2CO_3{\cdot}10H_2O$

The feasibility to produce crystals using a membrane contactor has been proved. However, still, some additional studies should be performed. Membrane scaling due to the deposition of crystals on the surface was observed in some experiments, mainly because of the recirculation of the feed stream, which introduced micro-crystals coming from the feed reservoir. The simple experimental setup used in this work should be completed with a crystallization reservoir after the membrane contactor and a pre-filtration of the recycle stream.

5. Conclusions

Osmotic membrane distillation-crystallization to obtain $Na_2CO_3{\cdot}10H_2O$ as a solid product was studied in this work. The evaluation of the system performance was carried out by varying the main operating conditions: flow rates and concentration of both feed and osmotic solutions and the feed temperature. On the one hand, feed flow rates under 50 mL min^{-1} revealed low turbulence and therefore, the polarization phenomenon appeared. On the other hand, it was demonstrated that the osmotic concentration has a higher influence in the transmembrane flux than the feed concentration due to the water activity difference. However, a higher driving force does not involve a better membrane performance. High concentration in the osmotic solution led to higher fluxes but the overall membrane coefficient did not increase as expected. A possible phenomenon of concentration polarization and/or membrane wetting could explain this loss of performance. An increase of temperature enhanced the flux but again, the mass transfer coefficient was not improved due to temperature polarization. The values of the overall mass transfer coefficient ranged between 4.34×10^{-12} m s^{-1} Pa^{-1} and 6.53×10^{-11} m s^{-1} Pa^{-1} for all the experiments collected in this work. The heat transfer coefficient was also obtained, ranging between 255.75 and 262.46 W m^{-2}. The heat fluxes increased with the osmotic concentration and the feed temperatures.

The resistance-in-series model was applied to compare the theoretical mass and heat transfer coefficients with the experimental ones with differences below 11.5%. In addition, the results allow concluding that the membrane represents the main resistance to the mass transfer. In the case of the heat transfer the main resistance is offered by the permeate side.

Finally, $Na_2CO_3{\cdot}10H_2O$ crystals were successfully obtained and a 65.6 ± 0.7 % of water content was found in the crystals.

This work demonstrates the feasibility to crystallize $Na_2CO_3{\cdot}10H_2O$ using a membrane contactor, including the mass and heat analysis, which are essential for further application of the technology as final step in a CO_2 capture scenario. Special attention to the membrane performance should be considered at higher temperatures and very concentrated osmotic solutions. An economic evaluation is essential to determine the best operating conditions.

Acknowledgements

I. Ruiz Salmón would like to acknowledge the support of the research group Ecoefficient Processes for Sustainable Industrial Chemical and Biochemical Engineering in the department of Materials and process engineering (IMAP) of the Institute of Mechanics, Materials and Civil Engineering (iMMC), at the Université catholique de Louvain. The authors acknowledge the financial support by the Fonds spéciaux de recherche (FSR) of the Université catholique de Louvain.

Appendix A

Water activities of the feed and osmotic solutions at different temperatures (Fig. A2) obtained by means of the sequence described by Sandler [19].

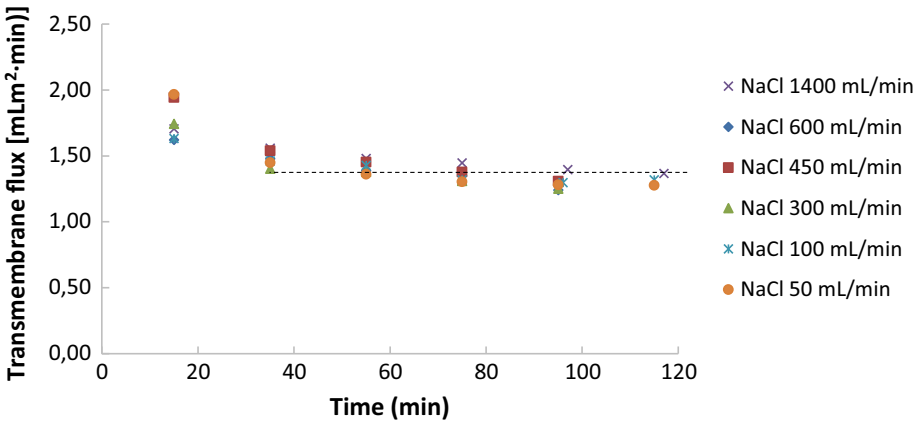

Fig. A1. Transmembrane flux as a function of time. The horizontal line indicates the steady state conditions.

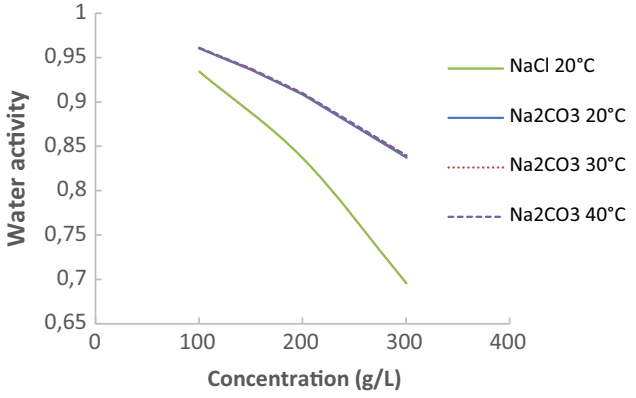

Fig. A2. Water activities in function of the concentration.

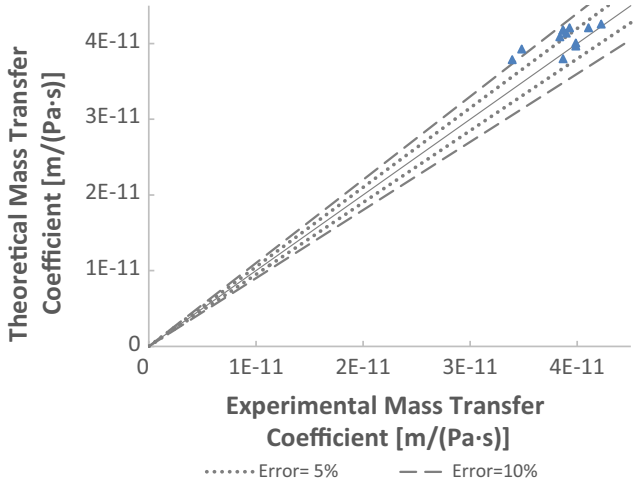

Fig. A3. Comparison of theoretical and experimental mass transfer coefficients. Na_2CO_3 and NaCl concentration are 150 and 300 g L^{-1}, respectively. Feed and osmotic flow rates ranges are 15–500 and 50–1400 mL min^{-1}, respectively.

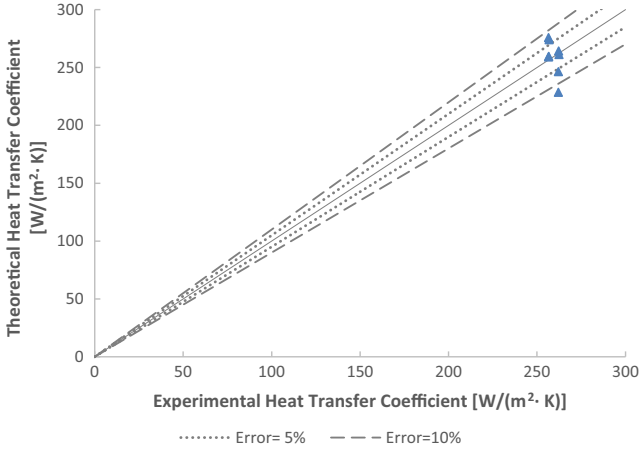

Fig. A4. Comparison of theoretical and experimental heat transfer coefficients. Na_2CO_3 concentration is 150 g L^{-1}. Feed and osmotic flow rates are 250 mL min^{-1}. NaCl concentration and temperature ranges are 200–300 g L^{-1} and 20–40 °C, respectively.

References

[1] J.T. Houghton, Y. Ding, D.J. Griggs, M. Noguer, P.J. van der Linden, X. Dai, K. Maskell, C.A. Johnson (Eds.), Climate Change 2001: The Scientific Basis. Contribution of Working Group I to the Third Assessment Report of the Intergovernmental Panel on Climate Change, Cambridge University Press, Cambridge, United Kingdom and New York, NY, USA, 2001.

[2] S. Solomon, D. Qin, M. Manning, Z. Chen, M. Marquis, K.B. Averyt, M. Tignor, H.L. Miller (Eds.), Climate Change 2007: The Physical Science Basis: Contribution of Working Group I to the Fourth Assessment Report of the Intergovernmental Panel on Climate Change, Cambridge University Press, Cambridge, United Kingdom and New York, NY, USA, 2007.

[3] NASA Jet Propulsion Laboratory, <http://climate.nasa.gov/400ppmquotes/>, 2016 (accessed 16.02.16).

[4] J.G. Olivier, Trends in global CO_2 emissions: 2013 Report. <http://edgar.jrc.ec.europa.eu/news_docs/pbl-2013-trends-in-global-co2-emissions-2013-report-1148.pdf>, 2013 (accessed 16.02.16).

[5] L.M. Romeo, I. Bolea, Overview post-combustion CO_2 capture, Boletín del Grupo Español del Carbón 35 (2015) 8–11.

[6] E. Favre, Membrane processes and postcombustion carbon dioxide capture: challenges and prospects, Chem. Eng. J. 171 (2011) 782–793.

[7] N. Verma, A. Verma, Amine system problems arising from heat stable salts and solutions to improve system performance, Fuel Process Technol. 90 (2009) 483–489.

[8] P. Luis, B. Van der Bruggen, The role of membranes in post-combustion CO_2 capture, Greenhouse Gases Sci. Technol. 3 (2013) 318–337.

[9] N. Keramati, A. Moheb, M.R. Ehsani, Effect of operating parameters on NaOH recovery from waste stream of Merox tower using membrane systems: electrodialysis and electrodeionization processes, Desalination 259 (2010) 97–102.

[10] K. Ghyselbrecht, M. Huygebaert, B. Van der Bruggen, R. Ballet, B. Meesschaert, L. Pinoy, Desalination of an industrial saline water with conventional and bipolar membrane electrodialysis, Desalination 318 (2013) 9–18.

[11] W. Kordylewski, D. Sawicka, T. Falkowski, Laboratory tests on the efficiency of carbon dioxide capture from gases in NaOH solutions, J. Ecol. Eng. 14 (2013) 54–62.

[12] U.S. Geological Survey, Mineral Commodity Summaries, <http://minerals.usgs.gov/minerals/pubs/commodity/soda_ash/mcs-2015-sodaa.pdf>, 2015 (accessed 16.02.16).

[13] T. Bakharev, J.G. Sanjayan, Y.B. Cheng, Alkali activation of Australian slag cements, Cem. Concr. Res. 29 (1999) 113–120.

[14] P. Luis, D. Van Aubel, B. Van der Bruggen, Technical viability and exergy analysis of membrane crystallization: closing the loop of CO_2 sequestration, Int. J. Greenhouse Gas Control 12 (2013) 450–459.

[15] B.R. Babu, N.K. Rastogi, K.S.M.S. Raghavarao, Mass transfer in osmotic membrane distillation of phycocyanin colorant and sweet-lime juice, J. Memb. Sci. 272 (2006) 58–69.

[16] W. Ye, J. Lin, J. Shen, P. Luis, B. Van der Bruggen, Membrane crystallization of sodium carbonate for carbon dioxide recovery: effect of impurities on the crystal morphology, Cryst. Growth Des. 13 (2013) 2362–2372.

[17] J.L. Li, B.H. Chen, Review of CO_2 absorption using chemical solvents in hollow fiber membrane contactors, Sep. Purif. Technol. 41 (2005) 109–122.

[18] W. Li, B. Van der Bruggen, P. Luis, Integration of reverse osmosis and membrane crystallization for sodium sulphate recovery, Chem. Eng. Process. Process Intensif. 85 (2014) 57–68.

[19] S.I. Sandler, Chemical, Biochemical, and Engineering Thermodynamics, fourth ed., John Wiley & Sons, USA, 2006.

[20] M. Brito Martínez, N. Jullok, Z.R. Negrín, B. Van der Bruggen, P. Luis, Membrane crystallization for the recovery of a pharmaceutical compound from waste streams, Chem. Eng. Res. Des. 92 (2014) 264–272.

[21] M. Gryta, M. Tomaszewska, A.W. Morawski, Membrane distillation with laminar flow, Sep. Purif. Technol. 11 (1997) 93–101.

[22] A.A.H. Al-Anezi, A.O. Sharif, M.I. Sanduk, A.R. Khan, Experimental investigation of heat and mass transfer in tubular membrane distillation module for desalination, ISRN Chem. Eng. (2012).

[23] A. Gabelman, S.T. Hwang, Hollow fiber membrane contactors, J. Memb. Sci. 159 (1999) 61–106.

[24] C.M. Tun, A.G. Fane, J.T. Matheickal, R. Sheikholeslami, Membrane distillation crystallization of concentrated salts—flux and crystal formation, J. Memb. Sci. 257 (2005) 144–155.

[25] A. Alkhudhiri, N. Darwish, N. Hilal, Membrane distillation: a comprehensive review, Desalination 287 (2012) 2–18.

[26] K.W. Lawson, D.R. Lloyd, Membrane distillation, J. Memb. Sci. 124 (1997) 1–25.

[27] D.M. Warsinger, J. Swaminathan, E. Guillen-Burrieza, H.A. Arafat, Scaling and fouling in membrane distillation for desalination applications: a review, Desalination 356 (2015) 294–313.

[28] L.D. Tijing, Y.C. Woo, J.S. Choi, S. Lee, S.H. Kim, H.K. Shon, Fouling and its control in membrane distillation—a review, J. Memb. Sci. 475 (2015) 215–244.

[29] K.W. Lawson, D.R. Lloyd, Membrane distillation. II. Direct contact MD., J. Memb. Sci. 120 (1996) 123–133.

[30] F. Laganà, G. Barbieri, E. Drioli, Direct contact membrane distillation: modelling and concentration experiments, J. Memb. Sci. 166 (2000) 1–11.

[31] General Chemical Industrial Products, SODA ASH. Technical & Handling Guide, <http://www.genchem.com/pdf/sodaashtech.pdf>, (accessed 16.02.16).

[32] K. Kobe, T. Sheehy, Thermochemistry of sodium carbonate and its solutions, Ind. Eng. Chem. 40 (1948) 99–102.